CHAPTER 2

Effects of Dimple Configurations on Heat Transfer and Friction Factors for Air Flow Over Flat Plate Having Dimple Surface

2.1 Introduction

This chapter is the study to find an appropriate dimple shape which may offer optimal heat transfer performance. The numerical simulation of laminar and turbulent model is employed to simulate the air flow over the dimple surface. The effect of dimples shape; dimple geometries and dimple attack angle of the ellipsoidal dimple were investigated. The heat transfer coefficient, surface friction coefficient and the effectiveness of each parameter were obtained and reported.

2.2 Problem definition

2.2.1 Problem conditions and main assumptions

Figure 2.1 shows the test surface which single dimple indent is employed. The problem under consideration is an external air flow over the isothermal plate and has the following conditions.

- The fluid is air at 300 K.
- The entrance air velocity is varied from 1 to 4 m/s.
- A constant surface temperature of 400 K is applied to the dimple and plain surface.
- The surfaces are no-slip conditions.
- The air flow is assumed to be in a steady state in three-dimensional domain.

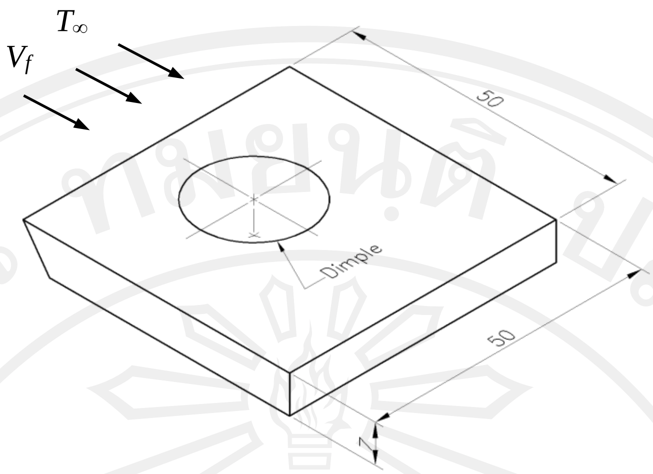

Figure 2.1 Details of dimple surface (all dimensions are in mm).

2.2.2 Numerical method

The numerical simulation of mixed convection of laminar and turbulent is obtained by using the SOLIDWORKS Flow Simulation 2012. The standard *k-ε* model (Launder and Spalding, 1974) is employed as the turbulence model for all numerical predictions. Figure 2.2 shows a side view of the computational grid which is employed for simulation. Number of cells in *x*, *y* and *z* direction is 112, 40 and 100 respectively, and the total computational cells are 448,700. The governing equations for the present system can be expressed by the following transport equations:

Continuity:

$$\frac{\partial \bar{u}_i}{\partial x_i} = 0 \tag{2.1}$$

Momentum:

$$\rho \bar{u}_j \frac{\partial \bar{u}_i}{\partial x_j} = -\frac{\partial \bar{p}}{\partial x_i} + \frac{\partial \bar{\sigma}_{ij}}{\partial x_j} - \frac{\partial \rho \overline{u_i' u'}}{\partial x_i} \tag{2.2}$$

Turbulent kinetic energy:

$$\rho \bar{u}_j \frac{\partial k}{\partial x_j} = G - \rho\varepsilon + \frac{\partial}{\partial x_j}\left[\left(\mu + \frac{\mu_t}{\sigma_k}\right)\frac{\partial k}{\partial x_j}\right] \tag{2.3}$$

Dissipation rate:

$$\rho \bar{u}_j \frac{\partial \varepsilon}{\partial x_j} = C_{\varepsilon 1}\frac{\varepsilon}{k}G - C_{\varepsilon 2}\frac{\varepsilon^2}{k} + \frac{\partial}{\partial x_j}\left[\left(\mu + \frac{\mu_t}{\sigma_\varepsilon}\right)\frac{\partial \varepsilon}{\partial x_j}\right] \tag{2.4}$$

Energy:

$$\rho \bar{u}_j \frac{\partial \bar{T}}{\partial x_j} = \frac{\partial}{\partial x_j}\left(\frac{\mu_t}{\Pr}\frac{\partial \bar{T}}{\partial x_j} - \overline{u_j' T'}\right) \tag{2.5}$$

Boussinesq approximation:

$$R_{ij} = -\frac{2}{3}\rho k \delta_{ij} + 2\mu_t \bar{s}_{ij} \tag{2.6}$$

where $R_{ij} = \rho \overline{u_i' u'}$, $\bar{\sigma}_{ij} = 2\mu \bar{s}_{ij}$, $\bar{s}_{ij} = \frac{1}{2}\left(\frac{\partial \bar{u}_i}{\partial x_j} + \frac{\partial \bar{u}_j}{\partial x_i}\right)$, $\mu_t = \rho C_\mu \frac{k^2}{\varepsilon}$, $C_\mu = 0.09$, $\sigma_k = 1.0$, $G = \mu_t\left(\frac{\partial \bar{u}_i}{\partial x_j} + \frac{\partial \bar{u}_j}{\partial x_i}\right)\frac{\partial \bar{u}_i}{\partial x_j}$, $C_{\varepsilon 1} = 1.44$, $C_{\varepsilon 2} = 1.83$ and $\sigma_\varepsilon = 1.3$

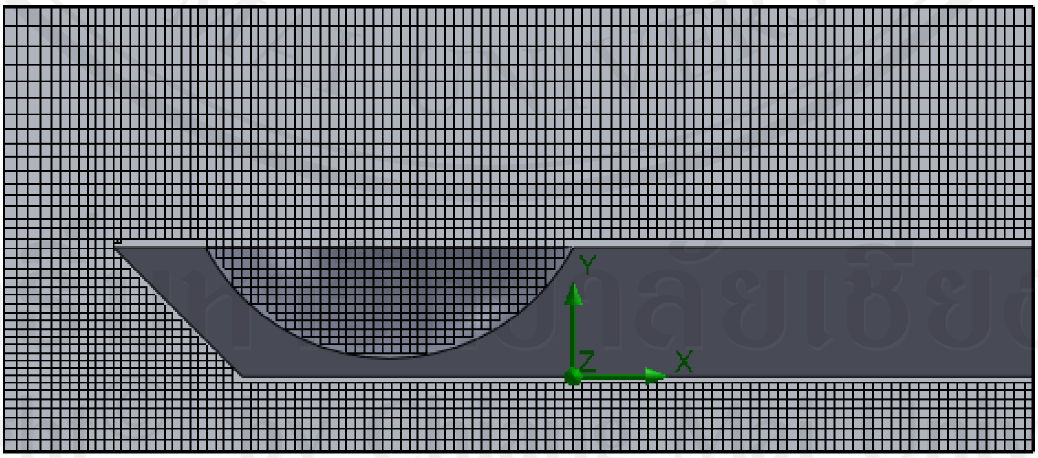

Figure 2.2 Computational grids for dimple surfaces.

2.3 Results and discussions

2.3.1 Data reduction

After simulation finished, the surface heat transfer rate and surface friction force are obtained to determine the heat transfer coefficient and surface friction coefficient. The average air side heat transfer coefficient (h) is calculated by

$$h = q''_s / (T_s - T_\infty) \tag{2.7}$$

where q'' is surface heat flux. The heat flux is calculated from heat rate level at the tested surface divided by the total surface area (flat portion and dimple surface), T_s is a surface temperature, and T_∞ is a temperature of inlet air stream flowing over the tested plate.

The average surface friction coefficient is calculated by

$$C_f = \frac{F_{s,x}}{\rho V_f^2 A / 2} \tag{2.8}$$

where $F_{s,x}$ is a surface friction force in x-direction, ρ and V_f are the density of air and air frontal velocity respectively. A is the total surface area (flat portion and dimple surface).

For comparing the integrated performance of dimple surface, an effectiveness (E) factor is obtained as the performance criterion. It is defined as the heat transfer ratio divided by the friction coefficient ratio.

$$E = (h/h_0)/(C_f/C_{f,0}) \tag{2.9}$$

where h_0 is an average air side heat transfer coefficient of flat plate, $C_{f,0}$ is an average surface friction coefficient of flat plate.

Reynolds number (Re_L) for air flow is defined as

$$\mathrm{Re}_L = \frac{\rho_f V_f L}{\mu_f} \tag{2.10}$$

where μ_f is the dynamic viscosity of air stream, L is a stream-wise surface length.

2.3.2 Result of base case

For setting up the numerical code, the heat transfer and pressure loss of external air flowing over the isothermal plain surface was simulated. The results are to be used as the bases when comparing with the dimple surface. The simulated results are shown in Figure 2.3.

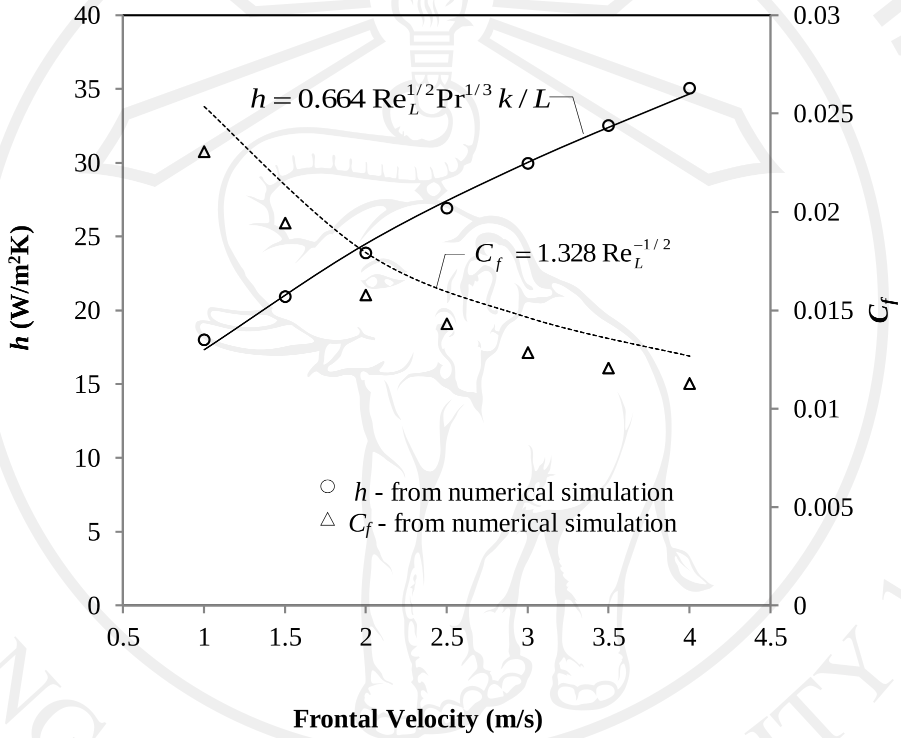

Figure 2.3 Comparison of the heat transfer coefficient and friction coefficient from the numerical simulation and the model.

From the Figure 2.3, average heat transfer coefficient values increase as frontal velocity increase. The average surface friction coefficient values decrease as frontal velocity increase vice versa. It is noticeable that the heat transfer coefficient data from the simulation agrees with the model. In respect of friction coefficient, although the result has an error about 10% base on the model, it showed the similar trend with the model.

2.3.3 Effect of dimple shape

In this part, there are three dimple configurations, spherical dimple, and two shapes of ellipsoidal dimple with 45° attack angle as shown in Figure 2.4.

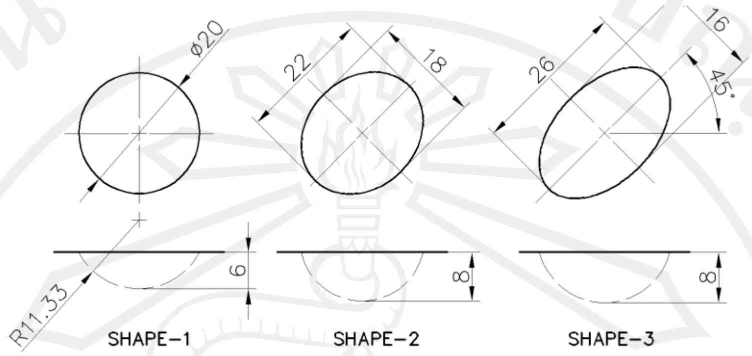

Figure 2.4 Dimple configurations.

Figure 2.5 shows the effect of dimple shape of the air side heat transfer performance. As shown in the figure, the h/h_0 values are less than 1.0 because in this study, only the performance of single dimple is evaluated. With reference to Katkhaw et al. (2014) explained that the heat transfer performance will be gradually adopted and increased at the next dimple along the streamline. From the simulated results, SHAPE-1 yields the highest heat transfer coefficient, in which is similar to Katkhaw et al.'s ones.

The effect of dimple shape to the surface friction coefficient is illustrated in Figure 2.6, where SHAPE-1 has the highest friction coefficient, SHAPE-2 and SHAPE-3 have the closer values similar to the heat transfer performance results shown in Figure 2.5.

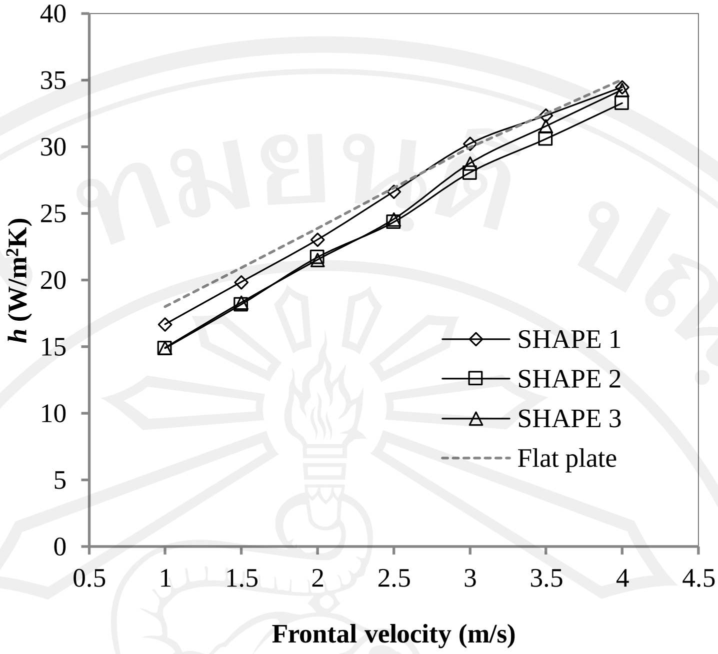

Figure 2.5 Effect of dimple shape to the air side heat transfer performance.

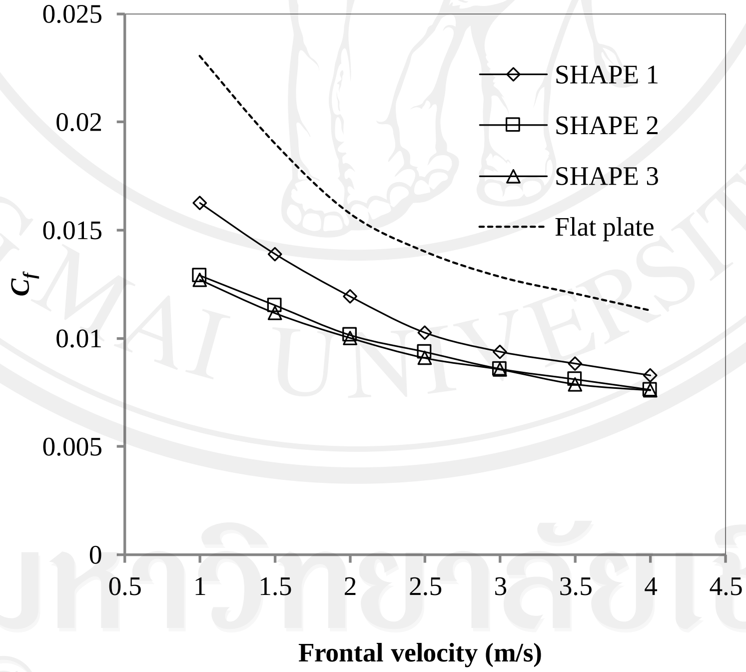

Figure 2.6 Effect of dimple shape to the surface friction coefficient.

Figure 2.7 shows the effect of dimple shape to the effectiveness (*E*). As shown in the figure, the SHAPE-3 gives higher effectiveness than other shapes in every frontal velocity.

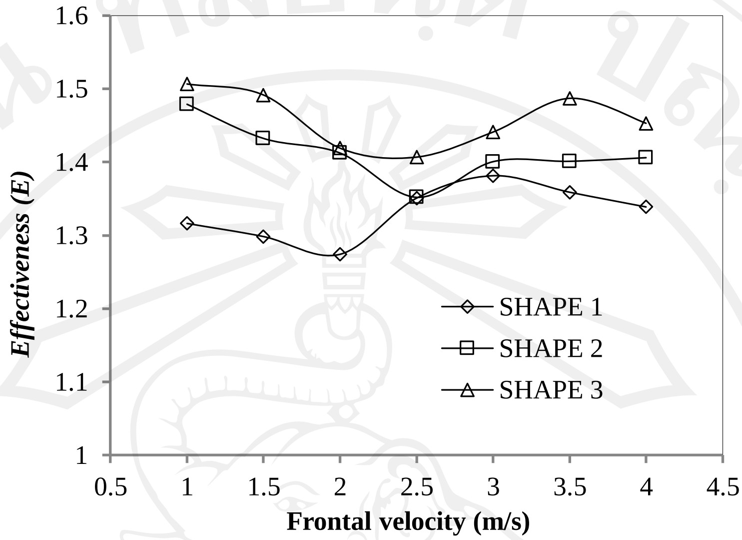

Figure 2.7 Effect of dimple shape to the effectiveness (*E*).

2.3.4 Effect of attack angle of dimple

In this part, the effect of the attack angle of 0^{o}, 30^{o}, 45^{o}, 60^{o}, and 90^{o} of ellipsoidal dimple surface is studied. Figure 2.8 shows the configuration of ellipsoidal dimples in different attack angles. See from the Figure 2.8, an air flow direction is from bottom to top.

The effect of attack angle on the air side heat transfer performance is illustrates in Figure 2.9. It shows that the heat transfer coefficient values decrease as the attack angles increase. This is because the small attack angles have a larger frontal area than the high attack angles.

Figure 2.10 shows the effect of the attack angle on the surface friction coefficient. The values decrease as the attack angles increase similar to the result of heat transfer performance, while the 90^{o} attack angle gives the values, considerably higher than other attack angles.

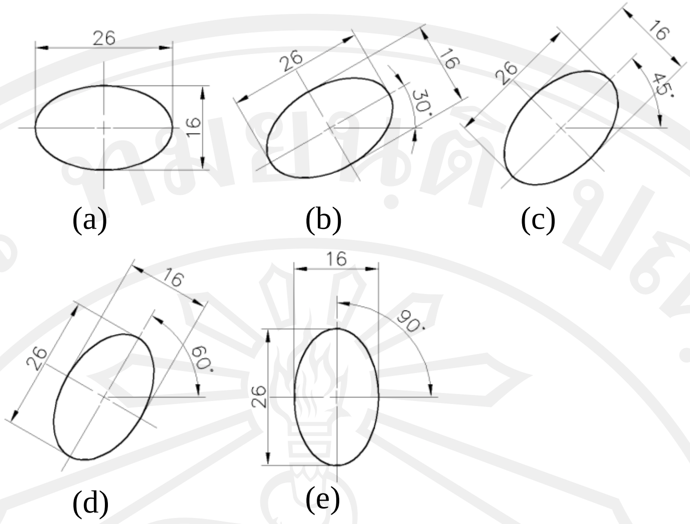

Figure 2.8 Details of: (a) 0^o attack angle (b) 35^o attack angle (c) 45^o attack angle (d) 60^o attack angle (e) 90^o attack angle.

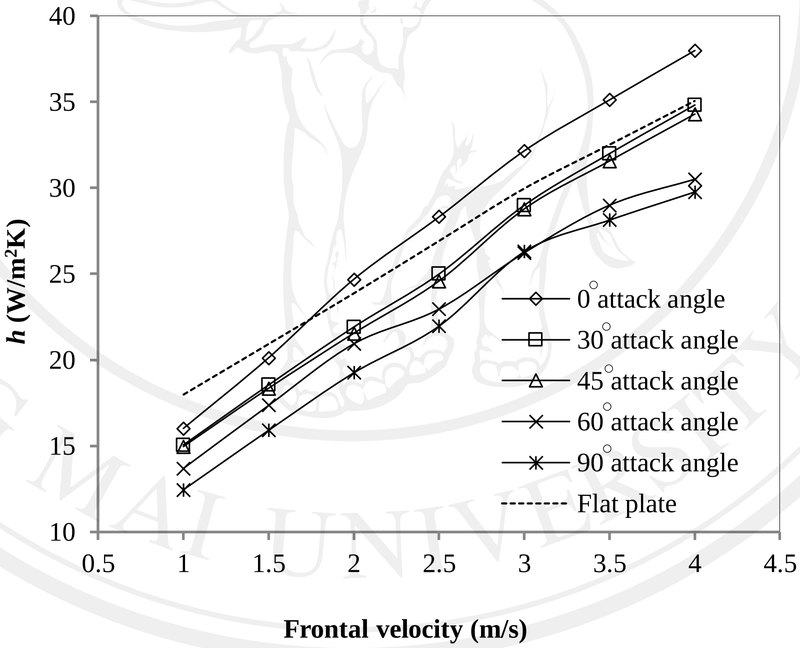

Figure 2.9 Effect of attack angle on the air side heat transfer performance.

The effectiveness (E) of each attack angles is illustrated in the Figure 2.11. As shown in the figure, the attack angle of 0^o gives an extremely low effectiveness and 45^o has the effectiveness, slightly higher than other attack angles.

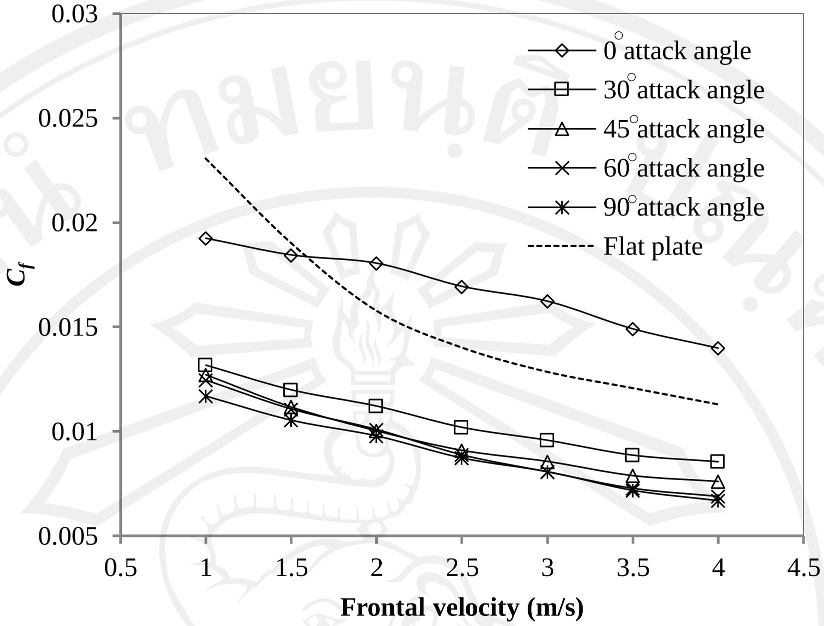

Figure 2.10 Effect of attack angle on the surface friction coefficient.

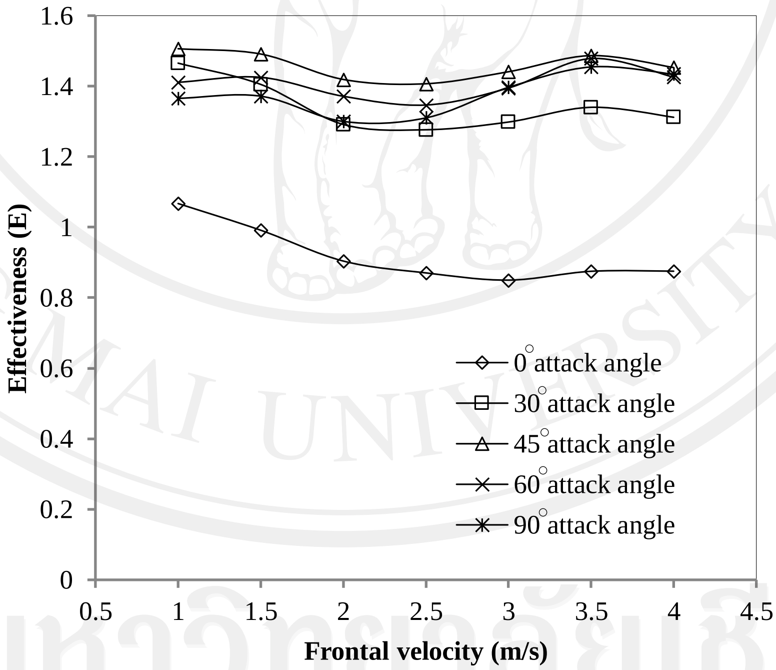

Figure 2.11 Effect of attack angles to the effectiveness (E).

2.4 Summary and conclusion

The present study reports on the heat transfer performance of air flow over the dimples surface. The effects of dimples shape, dimple attack angle and dimple depth are also examined. From the study, the conclusions are made as follows:

1) Spherical dimple surface gives the higher heat transfer performance than the ellipsoidal dimple. Nevertheless, ellipsoidal dimple surface gives the higher effectiveness (*E*) than the ellipsoidal dimple.

2) Both heat transfer performance and surface friction coefficient decrease as the attack angles increase, while the ellipsoidal dimple with 45^{o} attack angle gives the highest effectiveness (*E*).